Volume 25
Number 32
28 August 2023
Pages 4489–4612

# CrystEngComm

rsc.li/crystengcomm

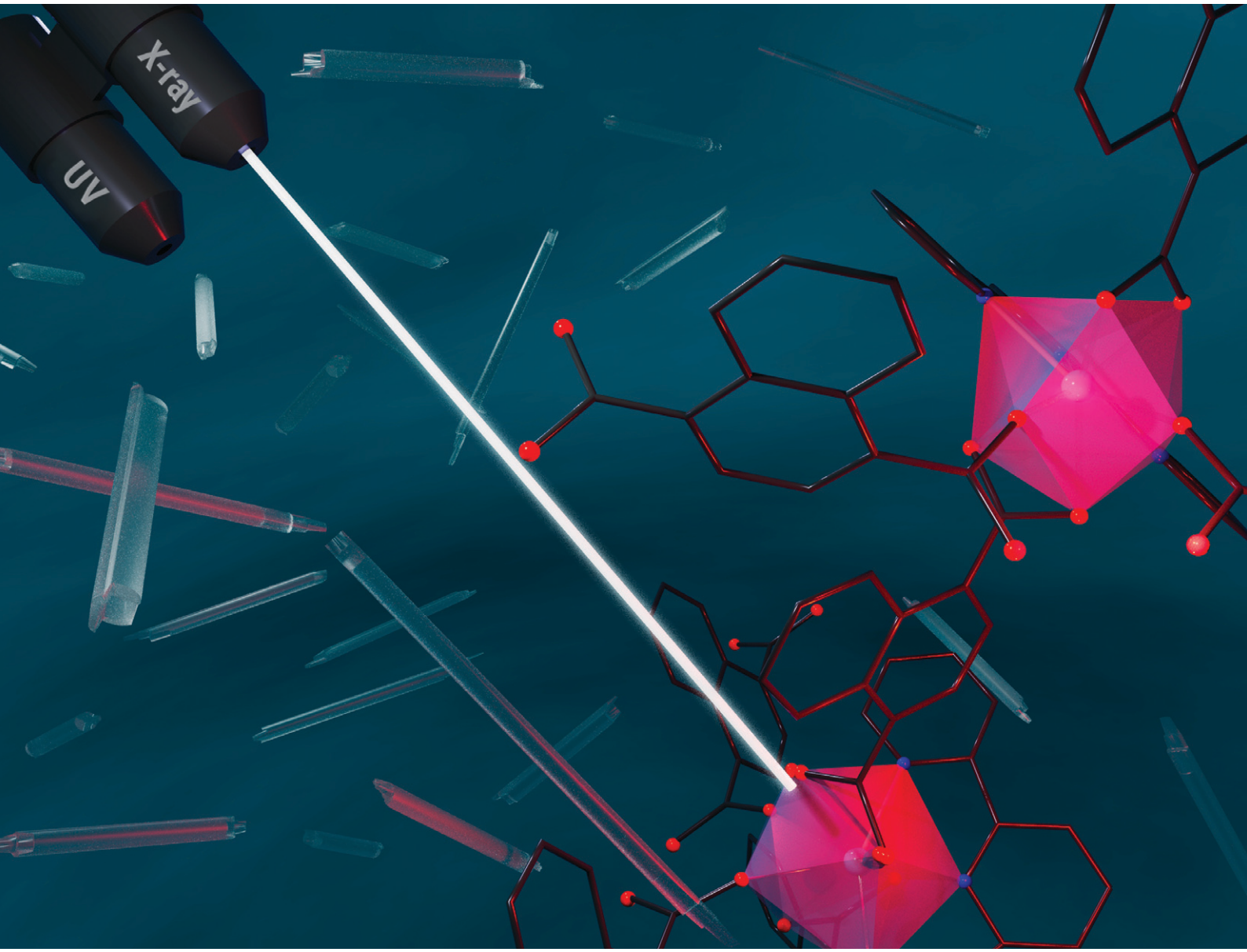


ISSN 1466-8033

ROYAL SOCIETY OF CHEMISTRY

**PAPER**
Robert G. Surbella *et al.*
Designing scintillating coordination polymers using a dual-ligand synthetic approach

CrystEngComm

PAPER

View Article Online
View Journal | View Issue



Cite this: *CrystEngComm*, 2023, **25**, 4496

# Designing scintillating coordination polymers using a dual-ligand synthetic approach†

Ana Arteaga, [a] Alice Lulich, [a] May Nyman [b] and Robert G. Surbella III *[a]

Herein we report the synthesis and structural characterization of three new europium containing coordination polymers: [Eu(terpy)(2,6-ndc)$_{1.5}$]·H$_2$O (Linus Pauling (LP) **1**), [Eu(terpy)(1,4-ndc)(1,4-Hndc)] (**LP-2**), and [Eu(phen)(2,6-ndc)$_{1.5}$]·DMF (**LP-3**). The title compounds were prepared hydro- or solvo-thermally and are constructed from either 1,4- or 2,6-naphthalenedicarboxylic acid (ndc) and 1,10-phenanthroline (phen) or 2,2′:6′,2″-terpyridine (terpy) ligands. The X-ray diffraction data show **LP-2** is two-dimensional while **LP-1** and **LP-3** are three-dimensional. Compounds **LP-1** and **LP-2** exhibit modest thermal stability up to 400 °C, while **LP-3** was notably unstable when removed from its reaction media and prone to degradation. Despite the apparent porosity, nitrogen physisorption measurements conducted on **LP-1** and **LP-2** revealed lower than anticipated surface area and pore volumes of 1 m$^2$ g$^{-1}$ and 0.037 cm$^3$ g$^{-1}$ and 1 m$^2$ g$^{-1}$ and 0.015 cm$^3$ g$^{-1}$, respectively. Photoluminescence characterization of all three compounds was performed in the solid state and in all cases the results reveal bright $Eu^{3+}$-based emission. The excitation spectra show the emissive properties arise from efficient ligand-to-metal resonance energy transfer. Additionally, **LP-1** and **LP-2** also display emission when exposed to soft X-rays, and as such show promise toward the design of scintillators.

Received 13th April 2023,
Accepted 3rd July 2023

DOI: 10.1039/d3ce00358b

rsc.li/crystengcomm



## Introduction

Lanthanide bearing coordination polymers (CP) and metal–organic frameworks (MOFs) continue to draw interest from the material science community owing to their promise in applications that span microelectronics, sensors, catalysis, and many others.[1–9] This breadth of functionality originates from the rich structural chemistry, and indeed diversity of reported structure types,[10–12] combined with the inherent electronic and physical properties of the 4f elements.[13] For example, the framework materials containing europium ($Eu^{3+}$) have garnered much attention for luminescence-based applications. Irradiation of such materials with a variety of excitation sources, such as ultraviolet light, X-rays, and α, β, and γ radiation (radioluminescence),[14,15] have resulted in bright metal-ion emission, as is the case for various chemical reactions (chemiluminescence)[16,17] and mechanical processess.[18–20] These properties have been broadly studied in multiple systems, including sol–gel glass, liquid crystals, and doped ceramics, for applications such as temperature indicators, barcoded materials,[21–23] and piezoelectric sensors.[24–29] Regardless of the application or underlying mechanism, maximizing the efficiency of the emissive process is of critical importance.

The molar absorptivity of the 4f–4f transitions that give rise to lanthanide luminescence are small because they are formally forbidden by the electronic selection rules.[30] Thus, direct excitation of the $Eu^{3+}$ metal ions (*via* the 4f–4f transitions) typically results in weak or inefficient luminescence emission. This is commonly overcome in small molecule and framework materials by sensitizing (or directly populating) the emissive state of the lanthanide ion *via* the antenna effect.[31,32] In short, an organic chromophore is leveraged to harvest photon energy that is used to populate the excited state of the metal ion through resonance energy transfer. This approach has been fruitful in preparing numerous lanthanide containing systems with high quantum efficiency.[33,34]

Recently we reported a series of lanthanide containing frameworks that were constructed of either chelating 1,10-phenanthroline (phen) or 2,2′:6′,2″-terpyridine (terpy) 'capping' ligands and 2,2′-bipyridine-4,4′-dicarboxylic acid (bpdc) ligand 'linkers'.[35] The combination of the phen and bpdc ligands was of particular note because the synthesized material was porous, and exhibited unique thermal

[a] *Pacific Northwest National Laboratory, 902 Battelle Boulevard, Richland, WA 99354, USA. E-mail: ana.arteaga@pnnl.gov, alice.lulich@pnnl.gov, robert.surbella@pnnl.gov*
[b] *Department of Chemistry, Oregon State University, 153 Gilbert Hall, Corvallis, Oregon 97331, USA. E-mail: may.nyman@oregonstate.edu*

† Electronic supplementary information (ESI) available. CCDC 2255873–2255875. For ESI and crystallographic data in CIF or other electronic format see DOI: https://doi.org/10.1039/d3ce00358b

properties and highly efficient $Eu^{3+}$-based emission. While there are a number of reported lanthanide/bpdc containing CPs and MOFs, many are of limited porosity.[36–38] The reason is that the spherical coordination environment of the lanthanide elements, when paired with a linear, bidentate ligand, (*e.g.*, bpdc), tends to promote dense or polycatenated structure types.[39,40] The dual-ligand approach has been recognized elsewhere as a potential path forward for promoting more open architectures.[41] Briefly, the chelating ligand will occupy one side of the metal center, disrupting the spherical coordination motif, while the second linear 'linker' ligand provides additional connectivity. The added steric bulk of the chelating ligand also has a secondary role in preventing the formation of dense interconnected frameworks or promoting connectivity *via* secondary noncovalent interactions.[42,43] Aside from these structural implications, the resulting material functionality tends to diversify, given that the properties of each ligand become integrated with those of the metal center.[44–47]

Herein we have explored the design of high dimensional network solids by leveraging a dual-ligand approach. The choice of the chelating phen and terpy ligands was strategic as both are known to be efficient sensitizers of the $Eu^{3+}$ emissive state.[30] The 1,4- and 2,6-naphthalenedicarboxylic acid (ndc) ligands were chosen not only for their role in luminescence sensitization, but also because similar species have been utilized in materials known to autoluminescent or function as an X-ray scintillator.[48] This synthetic approach led to the formation of three novel $Eu^{3+}$ bearing CPs: **LP-1**: $[Eu(terpy)(2,6\text{-ndc})_{1.5}]\cdot H_2O$, **LP-2**: $[Eu(1,4\text{-ndc})(1,4\text{-Hndc})(terpy)]$, **LP-3**: $[Eu(phen)(2,6\text{-ndc})_{1.5}]\cdot$DMF that all exhibit bright red $Eu^{3+}$-based emission. The X-ray diffraction data reveals the structure types are of two (**LP-1**) and three (**LP-2** and **LP-3**) dimensionalities and contain potential void spaces. The optical data reveal that luminescence properties stem from efficient ligand-to-metal resonance energy transfer. Notably, the study of the materials by powder X-ray diffraction (PXRD) reveal bright $Eu^{3+}$-based emission throughout the duration of the experiment with no signs of quenching or bleaching.

## Synthesis

The title compounds were synthesized hydro- or solvothermally within a 23 mL Teflon-lined acid digestion vessel. Europium chloride hexahydrate ($EuCl_3\cdot 6H_2O$) was combined with terpy and 2,6-ndc (**LP-1**) or 1,4-ndc (**LP-2**) in ultrapure water ($H_2O$). **LP-3** was synthesized by combining $EuCl_3\cdot 6H_2O$, phen and 2,6-ndc in dimethylformamide (DMF). The reactions were sealed and heated statically to 110 °C for 70 hours, and thereafter allowed to cool to room temperature. Crystals of **LP-1** were harvested from the mother liquor and were washed with ultrapure $H_2O$ and concentrated ammonium hydroxide. The material was then rinsed with ethanol and dried. Crystals of **LP-2** were washed with ethanol only. Compound **LP-3** was unstable in air and was therefore stored in fresh DMF. Single crystals of the title compounds were harvested from the bulk product and prepared for X-ray diffraction analysis (Table S1†). In addition, washed samples of **LP-1** and **LP-2** were characterized by PXRD, thermogravimetric analysis (TGA) and nitrogen physisorption measurements, attenuated total reflectance Fourier transform infrared spectroscopy (ATR-FTIR), diffuse reflectance (DR), and photoluminescence (PL) spectroscopies. The PL measurements for **LP-3** were performed on single crystals that were suspended within DMF. Additional synthetic and experimental details are provided in the ESI.†

## Results and discussion

### Crystal structure descriptions

Compound **LP-1**, $[(Eu(terpy)(2,6\text{-ndc})_{1.5})\cdot H_2O]$, crystallizes in the $P\bar{1}$ space group and features nine-coordinate metal centers, with each metal center bound to three nitrogen and six oxygen atoms to form a distorted tricapped trigonal prismatic geometry, with local $C_1$ symmetry, Fig. 1 and S2.† Each metal center is coordinated by one terpy ($\kappa^3$) and four total 2,6-ndc ligands. Two of the 2,6-ndc ligands feature bridging monodentate ($\mu_2$, $\kappa^1$) coordination while the others are ($\kappa^2$) chelating. The average $Eu^{3+}$–N and $Eu^{3+}$–O bond distances are 2.617(1) Å and 2.463(1) Å, respectively. The bond distances are typical for $Eu^{3+}$–N and $Eu^{3+}$–O bonds

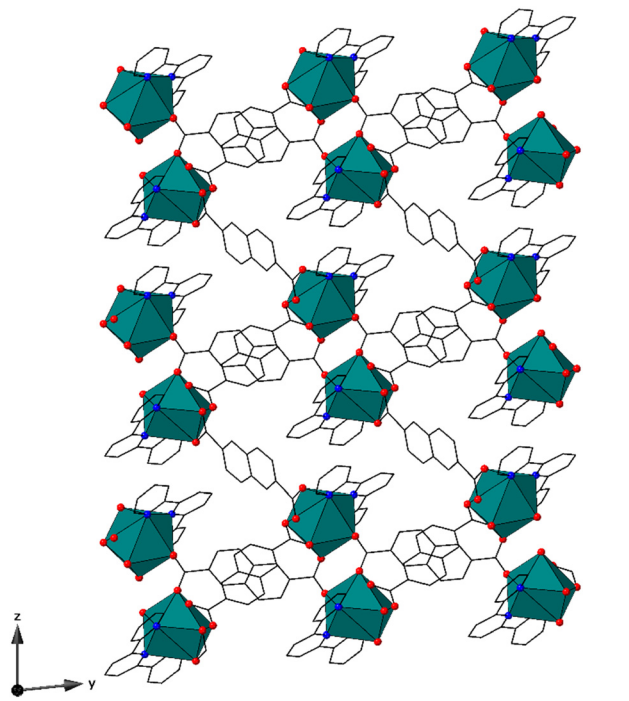


Fig. 1 The structure of **LP-1** is three-dimensional and contains small pores that propagate along the [100] direction. The $Eu^{3+}$ atoms are drawn as teal polyhedra. The O and N atoms are depicted as red and blue spheres, respectively, and the C atoms are represented by black sticks. The H atoms and solvent water molecules are omitted for clarity here and throughout this manuscript.

located within the Cambridge Crystallographic Data Centre (CCDC 2021.3.0, Mogul).[49] The 2,6-ndc ligands bridge the neighboring metal centers together, forming pseudo-dimeric units. Each unit is then linked to a total of four others, giving rise to a chain-like motif that propagates along the [010] direction. The chains are linked together by the 2,6-ndc ligands to form a porous three-dimensional structure type, with a mog type topology.[50–52] The pores feature 14 × 10 Å apertures and propagate along [100], and contain solvent water molecules.

Compound **LP-2**, [Eu(terpy)(1,4-ndc)(1,4-Hndc)], crystallizes in the $P2_1/n$ space group and contains nine-coordinate metal centers that feature a distorted tricapped trigonal prismatic geometry with approximate $C_2$ symmetry, Fig. 2 and S3.† Each $Eu^{3+}$ metal center is bound to three nitrogen and six oxygen atoms. The $Eu^{3+}$ metal centers are coordinated by one terpy ($\kappa^3$) and four total 1,4-ndc ligands, the latter in $\kappa^2$ chelating (two) and $\kappa^1$ (two) monodentate fashions. The average $Eu^{3+}$–N and $Eu^{3+}$–O bond distances are 2.571(2) Å and 2.438(2) Å. Similar to **LP-1**, the bond distances are unremarkable. The $\kappa^2$-1,4-ndc ligands connect the metal centers together to form sheets that span the (010) set of planes. The two $\kappa^1$-coordinating 1,4-ndc ligands are terminal and are oriented toward one another, creating a head-on C–H···O hydrogen bond motif. The terpy capping ligands form offset π-interactions with those from adjacent sheets to create a supramolecular three-dimensional network with a sql type topology.[50–52] The sheets are arranged such that they create potential void spaces in the [010] direction that feature ~11.5 × 7 Å apertures. Noncoordinated guest species were not located within the voids, and we note that the pore volume is small, comprising only 3% of the unit cell by volume.

Compound **LP-3**, [(Eu(phen)(2,6-ndc)$_{1.5}$)·DMF], crystallizes in the $P\bar{1}$ space group and contains eight-coordinate metal centers, with each metal center bound to two nitrogen and six oxygen atoms to form a distorted dodecahedral (bisdisphenoid) geometry with $C_1$ symmetry, Fig. 3 and S4.† Each metal center is coordinated by one phen ($\kappa^2$) and four 2,6-ndc ligands in $\mu_2$,- $\kappa^1$ monodenate bridging (two) and $\kappa^2$ chelating modes. The average $Eu^{3+}$–N and $Eu^{3+}$–O bond distances are 2.586(7) Å and 2.404(6) Å, respectively, and are within the expected range. The metal centers form dimeric nodes through linkages created by the 2,6-ndc ligands, similar to those in **LP-1**. These nodes are coordinated to a total of two others and form chain-like motifs that propagate along the [001] direction. The chains are linked together by the 2,6-ndc ligands to form a three-dimensional framework with potential voids (along [001]) that have 13 Å × 9 Å apertures, Fig. 3. The framework features a mog type topology.[50–52]

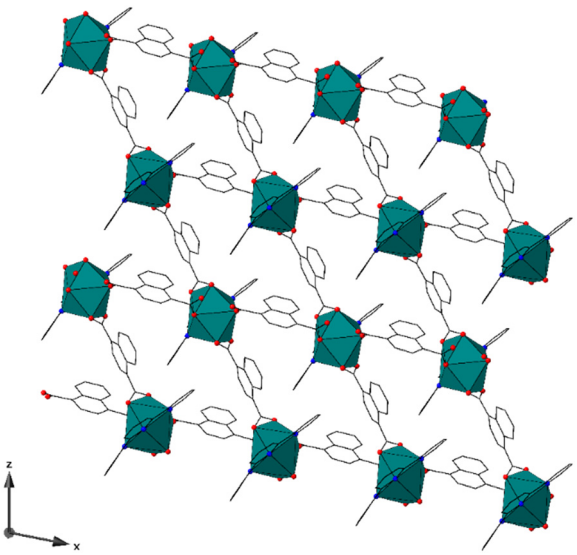


Fig. 2 Compound **LP-2** exhibits a two-dimensional structure type that contains potential void spaces along [010].

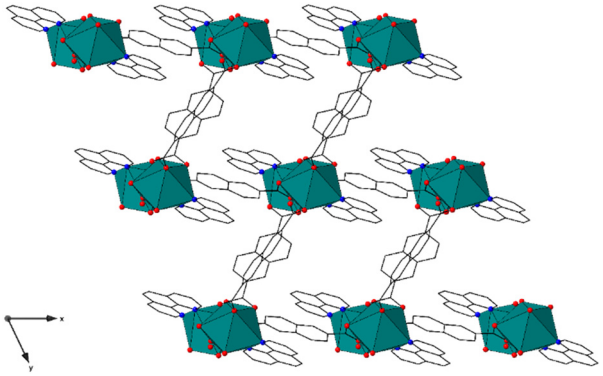


Fig. 3 The structure of **LP-3** is three-dimensional. The channels contain noncoordinated DMF guest species, which are not shown for clarity.

## Surface area analysis

Nitrogen gas physisorption measurements on **LP-1** and **LP-2** were conducted at 77 K to calculate surface area and pore volume, Fig. S5 and S6.† Powdered samples were analyzed after a 12 hour outgassing cycle at 100 °C under vacuum. The adsorption isotherm of **LP-1** reveals the Brunauer–Emmett–Teller (BET) surface area and pore volume are unexpectedly low at 1 $m^2\ g^{-1}$ and 0.037 $cm^3\ g^{-1}$, respectively. This result is surprising given that the three-dimensional structure of **LP-1** features 14 × 10 Å large apertures and potential void space that measures 1363 $Å^3$ per unit cell (as calculated using Platon).[53] The analysis of compound **LP-2**, a two-dimensional structure type with pseudo-pores (with 11.5 × 7 Å apertures) yields a similar result. The surface area and pore volume is 1 $m^2\ g^{-1}$and 0.015 $cm^3\ g^{-1}$, respectively. While these results were admittedly somewhat unexpected, we suspect the sterically large terpy capping ligands in **LP-1** and **LP-2** protrude into the pore spaces, and are responsible for the lower than expected surface area values. Attempts to remove the terpy ligands prior to analysis *via* thermal treatment to test this hypothesis were unsuccessful.

 

### Thermogravimetric analysis

The thermal stability of **LP-1** and **LP-2** were evaluated in air (21% $O_{2(g)}$) and $Ar_{(g)}$, Fig. S7.† The thermal decomposition of **LP-1** occurs in three distinct steps at temperatures of 290 °C, 435 °C, and 465 °C in air and 290 °C, 435 °C, and 605 °C in $Ar_{(g)}$. In each case, the first mass loss equates to about 5% by weight, which roughly correlates with four water molecules per unit cell, suggesting a mix of solvent and surface adhered species. The second and third decreases in mass are attributed to the decomposition of the terpy and 2,6-ndc ligands, respectively. Alternatively, **LP-2** decomposed in a two-step process, Fig. S7.† These steps occur at 365 °C and 450 °C in air and 365 °C and 580 °C in $Ar_{(g)}$. In both experiments, the first change in mass is attributed to the decomposition of the terpy ligands, while the second is the 1,4-ndc linker.

Experiments to explore the controlled (thermal) removal of the terpy ligands in **LP-2** was explored because of the modest window of stability (when compared to **LP-1**) that exists between 360–405 °C. A sample of **LP-2** was heated to 380 °C for 1 hour, and thereafter analyzed by PXRD, Fig. S9.† A total loss in material crystallinity was observed, indicating that the capping ligands could not be removed without compromising the crystal structure. This is not entirely surprising given the pore volume is small and not likely large enough to accommodate the loss of the bulky ligands. We point this out because in a past contribution we demonstrated in a similar material that the capping ligands could be post-synthetically removed thermally, with little effect on the crystallinity. This approach was used as a strategy for material activation, and had a measurable impact on the end-use of radionuclide sequestration.[35]

### Diffuse reflectance spectroscopy

The DR spectra of **LP-1** and **LP-2** were collected on powdered samples at room temperature, Fig. 4. Compound **LP-1** exhibits a strong, broad absorption feature below 370 nm that originates from the terpy and 2,6-ndc ligands. Superimposed are the $Eu^{3+}$-based 4f–4f transitions at 466, 526, 533, and 539 nm. These bands correspond to transitions between the $^7F_0$ and $^7F_1$ ground states and the $^5D_{1-2}$ excited states, Fig. 4.[30,54,55] The DR spectrum of **LP-2** is similar and dominated by a strong, broad absorbance band between 390 and 300 nm. Again, sharp $Eu^{3+}$-based 4f–4f transitions are present at 466, 526, 533, and 539 nm. The ligand-based absorption features were used to select the excitation wavelengths for the complementary PL measurements. The results for **LP-1** and **LP-2** were used to infer behavior for **LP-3**, which was not studied by DR.

### Photoluminescence spectroscopy

The title compounds were studied by PL spectroscopy using an excitation wavelength of 370 nm for **LP-1** and **LP-3**, and 390 nm for **LP-2**. Each material produced $Eu^{3+}$-based emission with the expected transitions from the $^5D_0$ excited state to the $^7F_{0-4}$ ground state manifold at 579

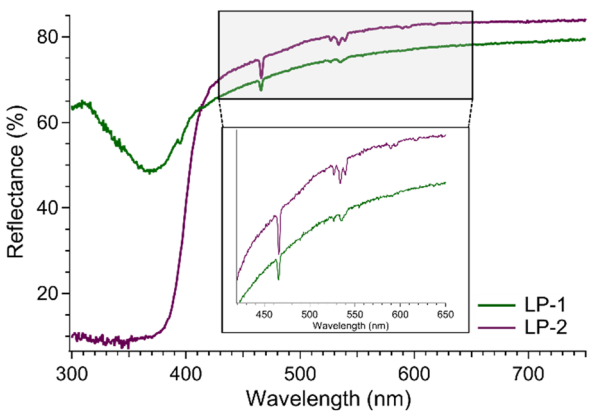


Fig. 4 DR spectra of **LP-1** and **LP-2** collected at 298 K on powdered samples.

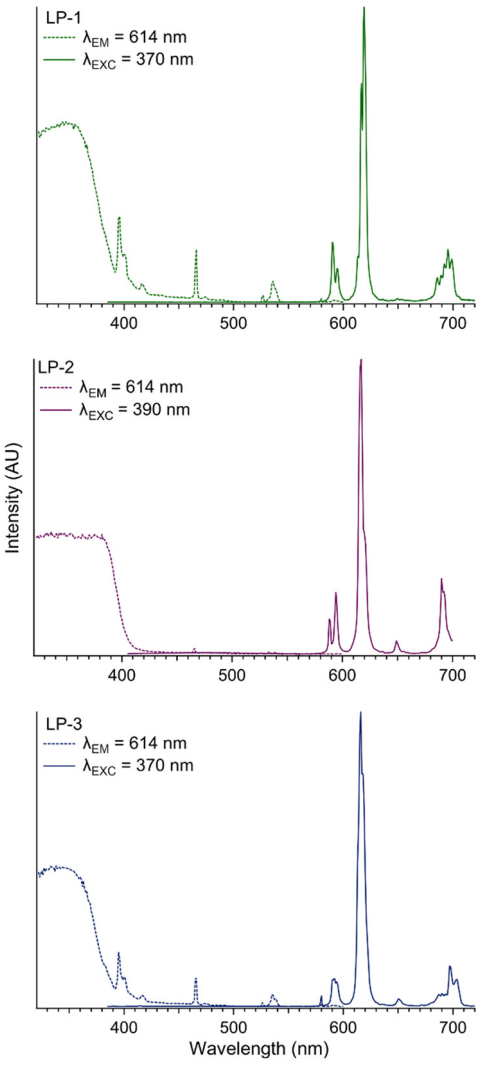


Fig. 5 The luminescence spectra of **LP-1**, **LP-2**, and **LP-3** collected at 298 K.

nm ($^7F_0$), 590 nm ($^7F_1$), 619 nm ($^7F_2$), 649 nm ($^7F_3$), and 695 nm ($^7F_4$), Fig. 5 and Table S2.†[55] Weak ligand-based emission is observed in **LP-2** only, suggesting efficient ligand-to-metal resonance energy transfer, Fig. S13.† Additional experiments on **LP-1–LP-3** conducted using an excitation wavelength of 466 nm (the $Eu^{3+}$ $^5D_2 \leftarrow {}^7F_0$ transition) results in a stark decrease to the emission intensity, further highlighting the effect of sensitization, Fig. S12–S14.† The excitation spectra of **LP-1–LP-3** were collected while monitoring the $^7F_2 \leftarrow {}^5D_0$ transition at 614 nm, Fig. 5 and Table S2.† Compounds **LP-1** and **LP-3** have similar excitation spectra, exhibiting strong ligand-based features between 320 and 380 nm and $Eu^{3+}$-based transitions at 395 nm ($^5L_6 \leftarrow {}^7F_0$), 416 nm ($^5D_3 \leftarrow {}^7F_0$), 466 nm ($^5D_2 \leftarrow {}^7F_0$), 526 nm ($^5D_1 \leftarrow {}^7F_0$), and 535 nm ($^5D_6 \leftarrow {}^7F_0$).[56] The excitation spectra of **LP-2** reveals the ligand contribution is red shifted related to **LP-1** and **LP-2**, and covers 324 to 399 nm. The $Eu^{3+}$-based transitions are again observed at 466 nm ($^5D_2 \leftarrow {}^7F_0$), 526 nm ($^5D_1 \leftarrow {}^7F_0$) and 535 nm ($^5D_6 \leftarrow {}^7F_1$). The red shift of the ligand absorption in **LP-2** is likely a result of the protonated 1,4-ndcH ligand in the crystal structure.[57] Luminescence lifetime data were collected on **LP-1** and **LP-2** only, Fig. S15 and S16,† and in each case the decay curves were fit with a monoexponential model. The results are $1.062 \times 10^{-3}$ s for **LP-1** and $1.001 \times 10^{-4}$ s for **LP-2**, suggesting the resonance energy transfer pathway in the former is more efficient.

### X-ray scintillation

Compounds **LP-1** and **LP-2** scintillate upon exposure to soft X-rays (Cu Kα, 8.04 keV). The result is bright pink emission that is visible to the naked eye, Fig. S17.† While reports of scintillating lanthanide containing CPs and framework materials are rising,[58–60] they remain underexplored and likely underreported. Published examples of lanthanide CPs that scintillate range in dimensionality and almost always feature $Eu^{3+}$ or $Tb^{3+}$ ions paired with aromatic chromophores.[35,61–65] For example, Wang *et al.* reported $Tb^{3+}$ and $Eu^{3+}$ isostructural scintillating CPs that were constructed from oxalate and phen ligands.[61] In the same study, a similar $Eu^{3+}$ CP that contained only the oxalate ligand did not exhibit analogous behavior; thus, the phen ligands are thought to serve an essential mechanistic role. It is hypothesized that the interaction of the $Eu^{3+}$ and $Tb^{3+}$ metal centers with the X-rays creates a fast electron (*i.e.*, the photoelectric effect) that is then transferred to the aromatic ligands. In turn, the ligands sensitize the emissive state of the metal centers *via* resonance energy transfer, causing either red ($Eu^{3+}$) or green ($Tb^{3+}$) emission. Here we note that reports of scintillating (or autoluminescent) compounds containing phen, terpy, and ndc have been reported.[6,35] The electronic origin of this phenomenon was not explored here, yet we note the blueprint for preparing these materials *a priori* is being developed.

## Conclusions

Presented here is the synthesis and structural characterization of three novel $Eu^{3+}$ containing CPs that were assembled using a dual-ligand synthetic approach. This strategy is proving effective for promoting higher dimensional network solids and preventing the formation of dense, interwoven structure types. Here, aromatic ligand chromophores were leveraged to sensitize the emissive states of the $Eu^{3+}$ metal centers, and as a result, the title compounds were highly luminescent and showed promise for X-ray detection. For the latter, the ligands are hypothesized to play important roles in the design of scintillating lanthanide containing framework materials. More broadly, these so-called designer frameworks are becoming more relevant given their promise towards applications that extend past fundamental science, and into commercial radiation detection.

## Author contributions

The manuscript was written with contributions from all authors.

## Conflicts of interest

There are no conflicts to declare.

## Acknowledgements

The primary funding mechanism for this study was the Laboratory Directed Research and Development Program at Pacific Northwest National Laboratory, a multiprogram national laboratory operated by Battelle for the Department of Energy. AA, AL, and RGS are all grateful for support from the Linus Pauling Distinguished Postdoctoral Fellowship. M. N. and A. A. acknowledges support from DOE's National Nuclear Security Administration (NNSA) for work conducted at Oregon State University, award number DE-NA0003763. The authors thank Michael A. Sinnwell for assistance in collecting the nitrogen physisorption measurements, guidance in assigning topological descriptors, and Santiago Alvarez for the helpful discussions on symmetry and geometry.

## References

1 J. A. Smith, M. A. Singh-Wilmot, K. P. Carter, C. L. Cahill and J. A. Ridenour, *Cryst. Growth Des.*, 2019, **19**, 305–319.
2 Y. Hasegawa and T. Nakanishi, *RSC Adv.*, 2015, **5**, 338–353.
3 S. A. Younis, N. Bhardwaj, S. K. Bhardwaj, K.-H. Kim and A. Deep, *Coord. Chem. Rev.*, 2021, **429**, 213620.
4 T. Gorai, W. Schmitt and T. Gunnlaugsson, *Dalton Trans.*, 2021, **50**, 770–784.
5 Y. Zhang, S. Liu, Z.-S. Zhao, Z. Wang, R. Zhang, L. Liu and Z.-B. Han, *Inorg. Chem. Front.*, 2021, **8**, 590–619.
6 H. Chen, J. Chen, M. Li, M. You, Q. Chen, M. Lin and H. Yang, *Sci. China: Chem.*, 2022, **65**, 2338–2350.

 

7 B. Li and B. Chen, in *Lanthanide Metal-Organic Frameworks*, ed. P. Cheng, Springer Berlin Heidelberg, Berlin, Heidelberg, 2015, pp. 75–107, DOI: 10.1007/430_2014_159.
8 S. Sahoo, S. Mondal and D. Sarma, *Coord. Chem. Rev.*, 2022, **470**, 214707.
9 Y. Hasegawa and Y. Kitagawa, *J. Photochem. Photobiol., C*, 2022, **51**, 100485.
10 B. Li, H.-M. Wen, Y. Cui, G. Qian and B. Chen, *Prog. Polym. Sci.*, 2015, **48**, 40–84.
11 S. Fordham, X. Wang, M. Bosch and H.-C. Zhou, in *Lanthanide Metal-Organic Frameworks*, ed. P. Cheng, Springer Berlin Heidelberg, Berlin, Heidelberg, 2015, pp. 1–27, DOI: 10.1007/430_2014_162.
12 A. M. Spokoyny, D. Kim, A. Sumrein and C. A. Mirkin, *Chem. Soc. Rev.*, 2009, **38**, 1218–1227.
13 K. P. Carter and C. L. Cahill, in *Handbook on the Physics and Chemistry of Rare Earths*, ed. J.-C. Bünzli and V. K. Pecharsky, Elsevier, 2015, vol. 47, pp. 147–208.
14 E. A. Seregina, A. A. Seregin and G. V. Tikhonov, *High Energy Chem.*, 2002, **36**, 223–228.
15 E. Zych, M. Wójtowicz, A. Dobrowolska and L. Kępiński, *Opt. Mater.*, 2009, **31**, 1764–1767.
16 M. Elbanowski, B. Mąkowska, K. Staninski and M. Kaczmarek, *J. Physiol. Pharmacol. Adv.*, 2000, **130**, 75–81.
17 M. Kaczmarek, *J. Lumin.*, 2020, **222**, 117174.
18 S. V. Eliseeva, D. N. Pleshkov, K. A. Lyssenko, L. S. Lepnev, J.-C. G. Bünzli and N. P. Kuzmina, *Inorg. Chem.*, 2010, **49**, 9300–9311.
19 Y. Hirai, T. Nakanishi, Y. Kitagawa, K. Fushimi, T. Seki, H. Ito and Y. Hasegawa, *Angew. Chem.*, 2017, **129**, 7277–7281.
20 Y. Hasegawa, R. Hieda, K. Miyata, T. Nakagawa and T. Kawai, *Eur. J. Inorg. Chem.*, 2011, **2011**, 4978–4984.
21 M.-L. Gao, W.-J. Wang, L. Liu, Z.-B. Han, N. Wei, X.-M. Cao and D.-Q. Yuan, *Inorg. Chem.*, 2017, **56**, 511–517.
22 Y. Zhang, S. Yuan, G. Day, X. Wang, X. Yang and H.-C. Zhou, *Coord. Chem. Rev.*, 2018, **354**, 28–45.
23 S. V. Eliseeva and J.-C. G. Bünzli, *Chem. Soc. Rev.*, 2010, **39**, 189–227.
24 H. R. Li, J. Lin, H. J. Zhang, L. S. Fu, Q. G. Meng and S. B. Wang, *Chem. Mater.*, 2002, **14**, 3651–3655.
25 K. Binnemans, P. Lenaerts, K. Driesen and C. Görller-Walrand, *J. Mater. Chem.*, 2004, **14**, 191–195.
26 K. Binnemans and C. Görller-Walrand, *Chem. Rev.*, 2002, **102**, 2303–2346.
27 P. Yan, Y. Qin, Z. Xu, F. Han, Y. Wang, Z. Wen, Y. Zhang and S. Zhang, *ACS Appl. Mater. Interfaces*, 2021, **13**, 54210–54216.
28 K. Li, E. Sun, Y. Zhang, Z. Song, X. Qi, Y. Sun, J. Li, B. Yang, J. Liu and W. Cao, *J. Mater. Chem. C*, 2021, **9**, 2426–2436.
29 Y. Zhai, J. Du, C. Chen, W. Li and J. Hao, *J. Alloys Compd.*, 2020, **829**, 154518.
30 K. Binnemans, *Coord. Chem. Rev.*, 2015, **295**, 1–45.
31 E. G. Moore, A. P. S. Samuel and K. N. Raymond, *Acc. Chem. Res.*, 2009, **42**, 542–552.
32 Y. Ma and Y. Wang, *Coord. Chem. Rev.*, 2010, **254**, 972–990.
33 E. E. S. Teotonio, G. M. Fett, H. F. Brito, W. M. Faustino, G. F. de Sá, M. C. F. C. Felinto and R. H. A. Santos, *J. Lumin.*, 2008, **128**, 190–198.
34 Y. Hasegawa, S. Tateno, M. Yamamoto, T. Nakanishi, Y. Kitagawa, T. Seki, H. Ito and K. Fushimi, *Chem. – Eur. J.*, 2017, **23**, 2666–2672.
35 R. G. Surbella III, D. D. Reilly, M. A. Sinnwell, B. K. McNamara, L. E. Sweet, J. M. Schwantes and P. K. Thallapally, *ACS Appl. Mater. Interfaces*, 2021, **13**, 45696–45707.
36 Z. Min, M. A. Singh-Wilmot, C. L. Cahill, M. Andrews and R. Taylor, *Eur. J. Inorg. Chem.*, 2012, **2012**, 4419–4426.
37 J.-Y. Wu, T.-T. Yeh, Y.-S. Wen, J. Twu and K.-L. Lu, *Cryst. Growth Des.*, 2006, **6**, 467–473.
38 R.-F. Li, Y.-W. Zhang, X.-F. Liu, X.-H. Chang and X. Feng, *Inorg. Chim. Acta*, 2020, **502**, 119370.
39 A. R. K. Chatenever, L. R. Warne, J. E. Matsuoka, S. J. Wang, E. W. Reinheimer, P. LeMagueres, H. Fei, X. Song and S. R. J. Oliver, *Cryst. Growth Des.*, 2019, **19**, 4854–4859.
40 X. Guo, G. Zhu, F. Sun, Z. Li, X. Zhao, X. Li, H. Wang and S. Qiu, *Inorg. Chem.*, 2006, **45**, 2581–2587.
41 K. P. Carter, C. H. F. Zulato, E. M. Rodrigues, S. J. A. Pope, F. A. Sigoli and C. L. Cahill, *Dalton Trans.*, 2015, **44**, 15843–15854.
42 H. He, D. Yuan, H. Ma, D. Sun, G. Zhang and H.-C. Zhou, *Inorg. Chem.*, 2010, **49**, 7605–7607.
43 J.-F. Qian, W.-J. Tian, S. Yang, Z.-H. Sun, L. Chen, M.-J. Wei, Z. Wu, M.-Y. He, Z.-H. Zhang and L. Mei, *Inorg. Chem.*, 2020, **59**, 17659–17670.
44 H. Dong, L. Zhao, Y. Chen, M. Li, W. Chen, Y. Wang, X. Wei, Y. Zhang, Y. Zhou and M. Xu, *Anal. Chem.*, 2022, **94**, 11940–11948.
45 L. Yu, L. Feng, L. Xiong, S. Li, Q. Xu, X. Pan and Y. Xiao, *ACS Appl. Mater. Interfaces*, 2021, **13**, 11646–11656.
46 Y.-Q. Sun, Y. Cheng and X.-B. Yin, *Anal. Chem.*, 2021, **93**, 3559–3566.
47 N. A. Ashashi, Z. U. Nisa, R. Singhaal, C. Sen, M. Ahmad, A. Frontera and H. N. Sheikh, *ACS Omega*, 2022, **7**, 41370–41391.
48 L. E. Kreno, K. Leong, O. K. Farha, M. Allendorf, R. P. Van Duyne and J. T. Hupp, *Chem. Rev.*, 2012, **112**, 1105–1125.
49 C. R. Groom, I. J. Bruno, M. P. Lightfoot and S. C. Ward, *Acta Crystallogr., Sect. B: Struct. Sci., Cryst. Eng. Mater.*, 2016, **72**, 171–179.
50 E. V. Alexandrov, A. P. Shevchenko and V. A. Blatov, *Cryst. Growth Des.*, 2019, **19**, 2604–2614.
51 V. A. Blatov, A. P. Shevchenko and D. M. Proserpio, *Cryst. Growth Des.*, 2014, **14**, 3576–3586.
52 M. O'Keeffe, M. A. Peskov, S. J. Ramsden and O. M. Yaghi, *Acc. Chem. Res.*, 2008, **41**, 1782–1789.
53 A. L. Spek, *Acta Crystallogr., Sect. D: Biol. Crystallogr.*, 2009, 148–155.
54 W. T. Carnall, P. R. Fields and K. Rajnak, *J. Chem. Phys.*, 1968, **49**, 4412–4423.
55 J.-C. G. Bünzli and S. V. Eliseeva, in *Lanthanide Luminescence: Photophysical, Analytical and Biological Aspects*, ed. P.

Hänninen and H. Härmä, Springer Berlin Heidelberg, Berlin, Heidelberg, 2011, pp. 1–45, DOI: 10.1007/4243_2010_3.
56 Z. Mu, Y. Hu, L. Chen, X. Wang, G. Ju, Z. Yang and R. Chen, *Ceram. Int.*, 2014, **40**, 2575–2579.
57 E. Badaeva, V. V. Albert, S. Kilina, A. Koposov, M. Sykora and S. Tretiak, *Phys. Chem. Chem. Phys.*, 2010, **12**, 8902–8913.
58 Z. Ajoyan, G. A. Mandl, P. R. Donnarumma, V. Quezada-Novoa, H. A. Bicalho, H. M. Titi, J. A. Capobianco and A. J. Howarth, *ACS Mater. Lett.*, 2022, **4**, 1025–1031.
59 W. Zhu, H. Yu, X. Zhu and H. Li, *Inorg. Chem. Commun.*, 2022, **136**, 109182.
60 X. Liu, R. Li, X. Xu, Y. Jiang, W. Zhu, Y. Yao, F. Li, X. Tao, S. Liu, W. Huang and Q. Zhao, *Adv. Mater.*, 2023, **35**, 2206741.
61 X. Wang, Y. Wang, Y. Wang, H. Liu, Y. Zhang, W. Liu, X. Wang and S. Wang, *Chem. Commun.*, 2020, **56**, 233–236.
62 A. Topor, D. Avram, R. Dascalu, C. Maxim, C. Tiseanu and M. Andruh, *Dalton Trans.*, 2021, **50**, 9881–9890.
63 Q. Gu, W. Wang, H. Lu, X. Chen, S. Wang and S. Wu, *Dalton Trans.*, 2022, **51**, 257–263.
64 J. Gao, J. Lu, B. Li, W. Wang, M. Xie, S. Wang, F. Zheng and G. Guo, *Chin. Chem. Lett.*, 2022, **33**, 5132–5136.
65 M. J. Neufeld, H. Winter, M. R. Landry, A. M. Goforth, S. Khan, G. Pratx and C. Sun, *ACS Appl. Mater. Interfaces*, 2020, **12**, 26943–26954.